Electrical properties of tholins and derived constraints on the Huygens landing site composition at the surface of Titan

Anthony Lethuillier, Alice Le Gall, Michel Hamelin, Sylvain Caujolle-Bert, Francis Schreiber, Nathalie Carrasco, Guy Cernogora, Cyril Szopa, Yann Brouet, Fernando Simões, et al.

Electrical properties of tholins and derived constraints on the Huygens landing site composition at the surface of Titan

A. Lethuillier[1], A. Le Gall[1], M. Hamelin[2], S. Caujolle-Bert[1], F. Schreiber[1], N. Carrasco[1], G. Cernogora[1], C. Szopa[1], Y. Brouet[3], F. Simoes[4], J.J. Correia[5], G. Ruffié[6]

[1]LATMOS/IPSL, UVSQ Universités Paris-Saclay, UPMC Univ. Paris 06, CNRS, 78280 Guyancourt, France.
[2]LATMOS/IPSL, UPMC Univ. Paris 06 Sorbonne Universités, UVSQ, CNRS, 75005 Paris, France.
[3]Physics Institute, University of Bern, Sidlerstrasse 5, CH-3012 Bern, Switzerland.
[4]Active Space Technologies, Parque Industrial de Taviero, 3045-508, Coimbra, Portugal.
[5]IPAG-CNRS, Université Grenoble Alpes, 38058 Grenoble, France.
[6]Bordeaux University, IMS Laboratory, IMS Transfert-A2M, ENSCBP, Pessac, France.

Key Points:

- The complex permittivity of tholins was measured in laboratory at low frequencies and low temperatures
- By comparison with measurements from Cassini/Huygens, constraints on the composition of the Huygens Landing Site are derived
- There is evidence for the presence of a conductive superficial layer at the Huygens Landing Site

Corresponding author: Anthony Lethuillier, anthony.lethuillier@latmos.ipsl.fr

Abstract

In 2005, the complex permittivity of the surface of Saturn's moon Titan was measured by the PWA-MIP/HASI (Permittivity Wave Altimetry-Mutual Impedance Probe/Huygens Atmospheric Structure Instrument) experiment on board the Huygens probe. The analysis of these measurements was recently refined but could not be interpreted in terms of composition due to the lack of knowledge on the low-frequency/low-temperature electrical properties of Titan's organic material, a likely key ingredient of the surface composition. In order to fill that gap, we developed a dedicated measurement bench and investigated the complex permittivity of analogs of Titan's organic aerosols called "tholins". These laboratory measurements, together with those performed in the microwave domain, are then used to derive constraints on the composition of Titan's first meter below the surface based on both the PWA-MIP/HASI and the Cassini Radar observations. Assuming a ternary mixture of water-ice, tholin-like dust and pores (filled or not with liquid methane), we find that at least 10% of water ice and 15% of porosity are required to explain observations. On the other hand, there should be at most 50-60% of organic dust. PWA-MIP/HASI measurements also suggest the presence of a thin conductive superficial layer at the Huygens landing site. Using accurate numerical simulations, we put constraints on the electrical conductivity of this layer as a function of its thickness (e.g., in the range 7-40 nS/m for a 7-mm thick layer). Potential candidates for the composition of this layer are discussed.

1 Introduction

On January 14, 2005, the Huygens probe [*Lebreton and Matson*, 2004], part of the Cassini/Huygens mission (NASA/ESA/ASI), landed on the surface of Titan, Saturn's biggest moon [*Lebreton et al.*, 2005]. After two hours and a half of descent, the probe touched a solid and possibly wet ground [*Zarnecki et al.*, 2005; *Atkinson et al.*, 2010] at a latitude of 10.3 °S and a longitude of 192.4°W [*Karkoschka et al.*, 2007]. While the measurements performed by the instruments on board Huygens cannot be regarded as representative of the entire surface of Titan, they do provide an important ground truth for the understanding of the observations of the Cassini orbiter or Earth-based telescopes.

Among the instruments on board the Huygens probe, a Mutual Impedance Probe (MIP), called PWA-MIP/HASI (Permittivity Wave Altimetry-Mutual Impedance Probe/Huygens Atmospheric Structure Instrument), measured for the first time the low-frequency (namely at 45, 90 and 360 Hz) electrical properties (i.e., the dielectric constant and electrical conductivity) of the first meter of Titan's surface [*Fulchignoni et al.*, 2005]. *Hamelin et al.* [2016] recently refined the analysis of the PWA-MIP/HASI observations, accounting for new insights on the final resting position of the Huygens capsule [*Schröder et al.*, 2012]. They inferred a dielectric constant of 2.5 ± 0.3 and a conductivity of 1.2 ± 0.6 nS/m at 45 Hz, values which are in agreement with previously published results but with much more reliable error bars. Following *Grard et al.* [2006], *Hamelin et al.* [2016] also reported that a sudden change in the electrical properties of the ground, namely a drop of its electrical conductivity, was recorded about 11 min after the Huygens landing. Several scenarios have been advanced to explain this event but more information on the electrical properties of materials relevant to Titan's surface at PWA-MIP/HASI frequencies are required to better understand PWA-MIP/HASI results in terms of near-surface composition and to conclude on the most plausible scenario for the observed sudden change in conductivity.

Prior to the Cassini mission, the composition of Titan's surface was thought to be that of its bulk crust i.e., dominated by water ice [*Tobie et al.*, 2005]. This was supported by the detection of water ice by *Griffith et al.* [2003] from telescope infrared spectroscopy measurements. However, since then, Cassini-Huygens observations have shown that water ice is only exposed at the surface of Titan at isolated locations including interdune corridors [*Barnes et al.*, 2008; *Le Gall et al.*, 2011] and crater rims [*Janssen et al.*, 2016]. In-

stead, the surface seems to be covered by a layer of organic materials, by-products of the intense photochemistry activity of Titan's atmosphere [*Clark et al.*, 2010; *Janssen et al.*, 2016].

The atmosphere of Titan is indeed the host of a complex photochemistry that produces a wealth of solid organic matter (or aerosols) by dissociation (mainly by solar UV rays) and recombination of the molecules N_2 and CH_4 [*Lorenz and Mitton*, 2002; *Waite et al.*, 2007]. The heaviest of these aerosols are eventually deposited onto the surface, progressively forming a thick sedimentary layer of organics. With time, surface processes (e.g., aeolian/pluvial/fluvial erosion, impacts, etc...) erode this layer and/or mix organics with water ice (see *Lopes et al.* [2010] for a review).

The present work aims at inferring new constraints on Titan's near-surface composition (in particular on its water-ice/organic mixture) from the electrical measurements made by PWA-MIP/HASI by comparison with laboratory measurements. While the electrical properties of water ice are well known [*Mattei et al.*, 2014], those of Titan's aerosols have never been measured at low frequencies in laboratory. In this paper, we present the measurement bench that we have developed to fill this gap. Measurements were performed on analogs of Titan's aerosols called "tholins" at a wide range of temperatures from room temperature down to almost 90 K. Measurements made at Titan's surface temperature (93.65 ± 0.25 K [*Fulchignoni et al.*, 2005]) were then used to better understand the implications of the PWA-MIP/HASI observations at the Huygens landing site (hereafter referred as to HLS).

2 Materials and Methods

2.1 Productions of tholins

The term "tholins" was introduced by *Sagan and Khare* [1979] to name the "brown, sometimes sticky, residue" they produced in laboratory at Cornell University by irradiating with various sources of energy a mixture of the cosmically abundant gases CH_4, C_2H_6, NH_3, H_2O, HCHO, and H_2S. The definition was later expanded to include many other components produced from different mixtures and even by irradiation of ices. It now seems that tholin-like materials are present in many bodies in the Solar System: on Pluto [*Grundy et al.*, 2016], Charon [*Grundy et al.*, 2016], comets [*McDonald et al.*, 1996; *Stern et al.*, 2015], Triton [*McDonald et al.*, 1994] and, of course, Titan [*Sagan et al.*, 1993].

Several set ups have been developed to synthesize and study analogs of planetary organic aerosols in laboratory (e.g., [*Szopa et al.*, 2006] [*Cable et al.*, 2012]). In particular, the PAMPRE (French acronym for Production d'Aérosols en Microgravité par Plasma REactifs – Aerosols Production in Microgravity by Reactive Plasma, [*Szopa et al.*, 2006]) experiment developed at LATMOS has been designed to reproduce the complex photochemistry of Titan's atmosphere. PAMPRE simulates the UV photolysis of N_2 and CH_4 and the induced photochemistry using a Capacitively Coupled Plasma (RF-CCP) discharge. This discharge is applied to a mixture of N_2 and CH_4 with a N_2/CH_4 ratio in the range 90/10 to 99/1, consistent with Titan's atmosphere composition at different altitudes [*Waite et al.*, 2007]. Inelastic electron impacts dissociate N_2 and CH_4 [*Szopa et al.*, 2006] and the resulting ions, neutral atoms and radicals recombine to form solid particles [*Carrasco et al.*, 2012]. The advantage of using a capacitive coupled RF plasma discharge is that the produced particles are in levitation between the two electrodes due to electrostatic forces and only deposit once they are heavy enough. This prevents them from interacting with the reactor walls that could act like a catalyst [*Szopa et al.*, 2006].

The PAMPRE-produced tholins are small spherical particles with a mean diameter between 0.093 and 1.070 μm [*Hadamcik et al.*, 2009]; they are regarded as possible analogs of Titan's organic aerosols. They form aggregates which can be observed micro-

scopically and have the macroscopic appearance of an orange powder (see Figure A.1) in agreement with the color of Titan's haze.

2.2 The PAP measurement bench

The central instrument of the PAP (French acronym for Permittivité d'Analogues Planétaires, permittivity of planetary analogs) measurement bench developed at LATMOS is a spectral analyzer (Solartron Modulab Material Test System©). The spectral analyzer uses a dipole system to generate an alternating current at frequencies in the range 1 Hz - 100 kHz between two electrodes separated by the cylindrical sample of material to be analyzed. The current and potential on the electrodes are then measured giving access to the complex impedance of the sample and thereby to its complex permittivity i.e., both its dielectric constant and electrical conductivity . The PAP electrodes are cylindrical with a radius of 10 mm and a height of 8 mm. An additional module was installed in order to measure currents down to the femto-Ampere which is necessary for materials with low dielectric constant and/or conductivity.

The PAP measurement bench also includes:

1. A mechanical press to produce samples of varying bulk density. Samples are shaped as cylinder pellets of 10 mm diameter with a height of 1 mm. A pressure of up to 8.8×10^8 Pa (maximum tonnage of 7 tons) can be applied to them.
2. A sample holder in which the electrodes and the sample are placed.
3. A pump to create vacuum (minimum 10^{-2} mbar) in the sample holder in order to prevent contamination by water ice (formed by condensation of the water in the air) of the sample when the temperature drops.
4. A cryostat to perform measurements at low temperatures. Cryogenic temperatures are reached by passive cooling, filling up with liquid nitrogen the reservoir in which the sample holder is placed. The temperature is recorded on both electrodes by PT100 temperature sensors. The temperatures recorded on the two electrodes are very close and we use the average of these two measurements to estimate the sample temperature. The lowest achievable temperature with this device is about 94 K, i.e. Titan's surface temperature at the HLS, and is obtained after ≈1 hr of cooling. After about 10 hrs all liquid nitrogen is evaporated and the temperature increases back to room temperature within about an additional 10 hrs. The temperature range for our measurements is therefore from 94 K up to room temperature.

The PAP set-up is designed to measure the complex permittivity of solid samples. In a harmonic regime and using complex notation, it is common to refer to the relative complex permittivity of the medium (i.e., relative to that of vacuum $\epsilon_0 = 8.854 \times 10^{-12}$ F/m) defined for fields and potentials in $exp(j\omega t)$ as follows:

$$\epsilon_r = \epsilon_r' - j\epsilon_r'' \tag{1}$$

The real part of the permittivity ϵ_r' (hereafter referred to as the dielectric constant) describes the polarizability of a material when an electrical field is applied. Its imaginary part ϵ_r'' is related to the electrical effective conductivity σ as follows: $\epsilon_r'' = \sigma / 2\pi f \epsilon_0$ with f the working frequency. We note that while pure dielectric materials have, by definition, a zero true conductivity (i.e., no free charge), polarization mechanisms induce the heat dissipation of electrical energy, which gives rise to a non-null effective conductivity.

The derivation of the complex permittivity from PAP measurements is described in Appendix A.

2.3 Description of the samples

The tholin samples were produced by the PAMPRE experiment for 3 different compositions of the initial gas mixture: 2%, 5% and 8% of CH_4. We investigated 15 samples i.e., 5 per composition totaling up to 300 hours of measurements most of which could be done unattended.

The material density of the tholins was measured using a helium pycnometer (Upyc-1200e-V5.04) which evaluates the volume occupied by a given sample with a known mass in a calibrated chamber by inserting helium gas in the chamber. The measured material densities (i.e. zero-porosity densities) are: $\rho_{tholins2\%} = 1.45 \pm 0.02$, $\rho_{tholins5\%} = 1.44 \pm 0.03$ and $\rho_{tholins8\%} = 1.34 \pm 0.03$. The porosity of the compressed samples measured with PAP can be readily inferred from these material densities. We find that the porosity of our samples is in the range 10-40%. Our experimental set up cannot produce samples with porosity out of this range. Samples with porosity >40% are too loose to be handled and placed in the sample holder. On the other hand, the mechanical press cannot compress further the samples. Of note, the material density values we found are consistent with those published by *Imanaka et al.* [2012] ($\rho_{tholins10\%} = 1.35 \pm 0.05$) but higher than those published by *Trainer et al.* [2006] ($\rho_{tholins} = 0.8 \pm 0.05$) and *Hörst and Tolbert* [2013] ($\rho_{tholins} \approx 0.5 - 1.15$). The difference in the experimental setup used to produce the tholins prevents a direct comparison although it seems that UV irradiation of CH_4 produces lower density tholins.

Futhermore, the composition of the initial gas mixture has an effect on the optical properties of the tholins; the higher the methane content the darker they appear. Additionally, the 2% samples were found to be less sticky and making pellets out of them proved to be more difficult than for the other compositions.

3 Complex permittivity of tholins

3.1 Effect of porosity

Figure A.2 shows the effect of porosity on the samples electrical properties. Overall and as expected, both the real and the imaginary parts of the permittivity decrease when porosity increases, vacuum having the lowest possible values of dielectric constant and conductivity (namely $\epsilon'_{r0} = 1$ and $\epsilon''_{r0} = 0$).

We use these measurements to determine the complex permittivity of the bulk tholins (i.e., with no porosity). This can be achieved by using a mixing law to "correct" the electrical properties of the investigated tholin samples for the contribution of vacuum. More specifically, we use the Maxwell-Garnett law [*Garnett*, 1904], which is the mixing law that best fits the data points presented in Figure A.2. This law relates the complex permittivity of the sample to its porosity p as follows:

$$\epsilon_{rsample} = \epsilon_{rm} + 3p\epsilon_{rm}\frac{1 - \epsilon_{rm}}{1 + 2\epsilon_{rm} - p(1 - \epsilon_{rm})} \tag{2}$$

where ϵ_{rm} is the bulk permittivity of tholins that can then be estimated by solving the second-degree equation:

$$2(p-1)\epsilon_{rm}^2(p\epsilon_{rsample} - 2p + 2\epsilon_{rm} - 1)\epsilon_{rm} + \epsilon_{rsample}(1-p) = 0 \tag{3}$$

The Maxwell-Garnett mixing law assumes that the void (spherical) pores (valid for $p < 0.5$) are smaller than the wavelength (300 m) which is readily achieved in our case. For example, at 94 K, 100 Hz and for a 5% methane composition the corrected complex permittivity is 4.5-j0.02.

3.2 Effect of frequency and temperature

Figure A.3 shows the complex permittivity of bulk tholins (i.e., once the correction described in section 3.1 has been applied) as a function of frequency and temperature for the three considered initial gas mixture compositions. The continuous lines and the shaded areas respectively represent the average and the standard deviation (at 2-σ) of the 5 samples measured per composition.

As expected, the dielectric constant increases with a decreasing frequency because polarization mechanisms have more time to take place when the applied electric field is slowly oscillating. Also the frequency dependence tends to disappear and the dielectric constant decreases when the temperature decreases i.e., when charge carriers become too slow to follow the applied electric field oscillations whether these oscillations are rapid or not. In particular, at Titan's surface temperature the dielectric constant seems to have reached its static limit.

The imaginary part of the complex permittivity displays a maximum at a frequency that moves towards lower values when the temperature decreases (1000 Hz at 220 K and 1 Hz at 170 K). The relaxation process at play may be a Maxwell-Wagner effect (i.e., interfacial polarization between the pores and the tholin matrix). At very low temperatures (in particular at 94 K), the relaxation peak is not visible anymore. Like for the real part, the imaginary part of the permittivity decreases with decreasing temperatures.

3.3 Effect of composition

We note a significant change in the electrical properties as a function of the composition of the gas mixture (i.e., the N_2/CH_4 ratio) from which they have been produced. The "5%-tholins" have the largest dielectric constant while the "8%-tholins" have the smallest (Figure A.4). This is true for all frequencies in the range 1 Hz-100 kHz.

For temperature in the range 125-225 K, the imaginary part of the permittivity of the tholins increases with an increasing methane proportion in the PAMPRE gas mixture. Outside this temperature range, the "2%-tholins" methane proportion still has the smallest imaginary part of the permittivity but the "5% tholins" has the largest (see Figure A.4). This is true for all frequencies in the range 1 Hz-100 kHz.

At 94 K and at a given frequency the dielectric constant varies by 0.5 and the imaginary part of the permittivity by 0.02 between the 3 studied compositions. This variation is larger than the accuracy of the spectral analyzer and higher than the dispersion of the measurements performed on multiple samples which gives us, in theory, the ability to distinguish between the different compositions.

Tholins show very low concentration of polycyclic aromatic hydrocarbons [*Derenne et al.*, 2012; *Mahjoub et al.*, 2016], therefore, the differences observed in the electrical properties are probably not due to the presence of aromatic components. *Mahjoub et al.* [2012] investigate the optical indices of tholins as a function of the methane percentage used in the initial gas mixture. They find that the 2% tholins are far more absorbant in the UV-visible than the 8% tholins and explain this difference by the quantity of nitrogen incorporated in the tholins, primarily in amines, which was found to be higher at low methane fraction in the initial gas. In amines, the nitrogen has a non-binding electrical doublet which results in a higher dielectric constant. This could explain the differences between the 8% and 5% tholins but the fact that the 2% tholins have a lower dielectric constant than the 5% suggests that additional unknown mechanisms influence the electrical properties.

The measured dielectric constant of tholins at low frequency is relatively close but different from that of water ice (3.15 at cryogenic temperatures [*Mattei et al.*, 2014]) or of Martian analog JSC-Mars-1 (2.0-2.5 at 220 K [*Simões et al.*, 2004]). Furthermore, at

low frequencies most rocky materials present on the Earth have a dielectric constant in the range 3.4 (dry sandy soil [*Clark*, 1966]) - 13.0 (sandstone [*Clark*, 1966]).

3.4 Dielectric relaxation model for tholins

One of the most commonly used models to represent the frequency dependence of the electrical properties of material is the Cole-Cole model with conduction [*Cole and Cole*, 1941]:

$$\epsilon_r(f,T) = \epsilon_\infty(T) + \frac{\epsilon_s(T) - \epsilon_\infty(T)}{1 + (j2\pi f\tau(T))^{1-\alpha}} - j\frac{\sigma_s}{2\pi f\epsilon_0} \quad (4)$$

where ϵ_∞ is the relative high-frequency limit permittivity, ϵ_s the static (low-frequency limit) relative permittivity, τ the relaxation time in seconds, σ_s the static conductivity and α an exponent representing the broadness of the relaxation transition. It is reduced to the Debye equation when $\alpha = 0$.

Figure A.5 shows the Cole-Cole model best fitting to our measurements in the complex plane (plotted with different scales for ϵ_r' and ϵ_r'') at a temperature of 94 K for tholins obtained with 5% of methane. The best-fit parameters are: $\epsilon_s = 4.24$, $\epsilon_\infty = 4.53$, $\tau = 2.0 \times 10^{-4}$ s, $\alpha = 0.84$, $\sigma_s = 0.0183$ S/m.

Complementary electrical characterization of tholins are available in literature (see Table 1). In particular, *Rodriguez et al.* [2003] and *Paillou et al.* [2008] measured the complex permittivity of tholins obtained from a 2% methane atmosphere in the Ku-band (namely at 10 and 13 GHz) and at 77 K to support the analysis of the Cassini Radar observations *Elachi et al.* [2004]. *Paillou et al.* [2008] reported a permittivity of 1.17-j0.0033 for a "non-compacted sample" of tholins and of 2.33-j0.0206 for a "compacted sample". These values are logically below the ones measured at lower frequencies as explained in section 3.2. It would have been useful to know the actual porosity of the samples investigated in the Ku-band in order to determine the permittivity of bulk tholins in this frequency range as we did in the 1 Hz-100 kHz domain (section 3.1). However, we do know that the "compacted samples" were obtained with a press tonnage of 15 t, which suggests that their porosity is at most 10 % [*Paillou*, personal communication] hence a maximum permittivity of 2.55-j0.025 based on the Maxwell-Garnett law. Interestingly, we note that the dielectric constant of tholins is larger than that of water ice at low frequencies while it is the opposite in the Ku-band.

More recently, *Brouet et al.* [2016] measured the dielectric constant of tholins synthesized from a 5% methane atmosphere in the frequency range 50 MHz-2 GHz but at a warm temperature of 243 K.

Therefore, contrary to water ice, tholins do not seem to fully lose the frequency dependence of their dielectric constant at very low temperature. The main polarization mechanism responsible for the dielectric constant of water ice is the reorientation of H_2O molecules. This mechanism is greatly affected by temperature and this explains why the dielectric constant of water ice loses its frequency dependence at temperature below about 150 K [*Mattei et al.*, 2014]. In the case of tholins, the polarization mechanisms at stake must be more complex and more numerous. Their investigation is out of scope of this paper.

4 Titan's subsurface composition at the Huygens Landing site

4.1 State of art: permittivity of Titan's near-surface, case of the HLS

The first estimate of the dielectric constant of Titan's near-surface was derived from observations from the Arecibo radar system: *Campbell et al.* [2003] found a range of di-

electric constants of 1.5-2.2 with a mean value of 1.8 for Titan's 26 °S latitude band (we recall that the Huygens landing site is at a latitude of 10.3 °S). After the arrival of the Cassini probe at Saturn, the Radar on board (operating at 13.78 GHz, *Elachi et al.* [2004]) provided new and spatially resolved constraints on the dielectric constants of Titan's near-surface both in its real-aperture active (scatterometry) and passive (radiometry) modes.

The analysis of the scatterometry data yields dielectric constants in the range 1.9-3.6 with a mean value of 2.2 [*Wye et al.*, 2007]. This analysis is based on raster scanning of large regions at a resolution of about 100 km. No comprehensive investigation of the dielectric constant of the HLS has been published yet. However, it probably exhibits a dielectric constant close to that measured in the plains of Titan, namely, 2.12 ± 0.07 [*Wye et al.*, 2007].

Radiometry insights into the surface dielectric constant come in two flavors. First, when the spacecraft is far away from Titan (25 000-100 000 km), the disk is scanned twice in two orthogonal polarizations (the spacecraft is rotated between the two scans). These polarization pairs can be used to produce a global map of the surface dielectric constant [*Janssen et al.*, 2009, 2016]. This map is essentially low resolution (300-500 km) except for a a few regions that could be observed in mid-resolution in the two orthogonal polarizations during two different flybys. This is fortunately the case of the HLS region for which the dielectric map has a resolution of about 100 km and indicates a value of 1.7 ± 0.2. For comparison, the global dielectric map displays values in the range 1.0 (no polarization plus some allowance for error)-2.25 with an average of 1.54.

Second, the radiometry observations collected at all resolutions (from 5 to 500 km) can be used to build a mosaic of Titan's surface emissivity at 2.2-cm at normal incidence [*Janssen et al.*, 2009, 2016]. The emissivity map has a resolution of about 5 km at the Huygens landing site, which has been observed several times at closest approach. It indicates an emissivity of 0.94 ± 0.01, which implies, if this region does not depart too much from a Kirchhoff surface, an effective dielectric constant of 2.7 ± 0.25.

The discrepancy between the effective relative permittivity derived from the polarized radiometry measurements (1.7 ± 0.2) and the effective relative permittivity derived from the emissivity at normal incidence (2.7 ± 0.25) suggests that Kirchhoff's approximation does not apply in general to the HLS region. Surface small-scale roughness or, more likely, volume scattering from the subsurface must be invoked in order to reconcile these two observations, although their different resolutions may play a part too. The average effective dielectric constant at 13.78 GHz of the Huygens landing site region must thus lie between 1.5 and 3.0 as also suggested by the scatterometry analysis.

The imaginary part of the complex permittivity of Titan's surface was not measured by the Cassini Radar/radiometer but the analysis of the seasonal thermal wave points to a mean 2.2-cm emission depth in the range 40–100 cm for the dominant radar-dark terrains, consistent with the value ϵ_r'' of tholins as measured by *Paillou et al.* [2008][*Janssen et al.*, 2016].

Lastly, the permittivity probe PWA-MIP/HASI on board the Huygens probe measured both the real and imaginary parts of the complex permittivity of the HLS in the EVL (Extremely and Very Low) frequency range. At 45 Hz (frequency for which the PWA-MIP calibration is best), *Hamelin et al.* [2016] found $\epsilon_r' = 2.55 \pm 0.35$ and ϵ_r'' in the interval $0.2 - 0.8$ for the first 11 min after the landing and $\epsilon_r' = 2.35 \pm 0.35$ and ϵ_r'' in the interval $0 - 0.1$ after. These values are consistent with the ones previously published [*Grard et al.*, 2006] but with more reliable error bars that account for uncertainties related to the probe's resting attitude on the surface.

More importantly, we highlight that the sounding depths of the Cassini Radar/radiometer and of PWA-MIP/HASI are similar: both instruments are sensitive to the composition and structure of, roughly, the first meter below the surface [*Hamelin et al.*, 2016; *Janssen et al.*,

2016]. More specifically, in the case of PWA-MIP/HASI it is a weighted volume average of the first meter with a weight decreasing with depth (for a more in depth discussion see *Lethuillier* [2016]). All the observations mentioned above are reported in Table 2. They are further discussed in the following section.

4.2 Constraints on the composition of the HLS from dielectric measurements

Based on the values presented in Table 2 and assuming that they are all representative of the HLS, we put some constraints on the composition of the subsurface in this region.

The range of permittivity values reported in section 4.1 is consistent with the expected dielectric constants of materials relevant to Titan (see Table 1). More specifically, permittivity values derived from microwave observations overlap those of solid and liquid hydrocarbons. They preclude solid sheets of water ice but not water ice in a porous form. Indeed, we highlight that the values reported above are effective dielectric constants; they depend on both the composition and physical state of the surface/subsurface. In particular, they are affected by the subsurface porosity. As a consequence, microwave observations do not proscribe a fractured, porous water ice surface which would exhibit an effective dielectric constant much smaller than 3.15, the dielectric constant of bulk water ice. Likewise, while low-frequency observations preclude a compacted layer of tholin-like organics they do allow tholins as part of the near-surface composition. Assuming that the composition of the first meter below the surface is a ternary mixture of water ice, tholin dust and pores (empty, partially or fully filled with liquid methane), we use both microwave and PWA-MIP/HASI results to constrain the respective proportion of these ingredients.

For that purpose, we also assume that Titan's tholins are similar to those synthesized in laboratory from a mixture 95/5 of N_2/CH_4 as this is the gas mixture that produces the largest abundance of solid aerosols [*Sciamma-O'Brien et al.*, 2010]. Further, based on the idea that the real part of the permittivity of liquid methane at 94 K should be identical at near-DC and microwave frequencies, we use the same value of 1.67 in both frequency domains as measured by *Leese et al.* [2012] at 100 Hz (see Table 1). Unfortunately, this latter assumption cannot be made for the imaginary part of the permittivity for which no measurement at PWA-MIP/HASI frequencies is available in literature. As a consequence, as long as the low-frequency electrical properties of liquid hydrocarbons are not investigated in laboratory, the PWA-MIP/HASI measurements of ϵ_r'' cannot be used to place constraints on the composition of Titan's near-surface. However, we highlight that the ϵ_r'' value measured by PWA-MIP/HASI just after landing (see Table 2) is larger, by one or even two orders of magnitude than the expected values for tholins and water ice (see Table 1). Since liquid hydrocarbons likely also have a small loss tangent (as measured in laboratory in the microwave domain (see Table 1) and shown to be true at the surface of Titan by *Mastrogiuseppe et al.* [2014]), PWA-MIP/HASI measurements suggest that an extra conductive material is present at the HLS. The removal of this material may explain the sudden drop of conductivity recorded 11 min after the Huygens landing. This hypothesis is further discussed in section 4.3.

Figure A.6 shows the lower and upper limits of the volumetric fractions of the three considered ingredients of the near-surface as derived from the microwave (red) and PWA-MIP/HASI (blue) observations using the Hashin-Shtrikman bounds of the Maxwell-Garnett mixing formula [*Hashin and Shtrikman*, 1962]. These limits are shown on ternary diagrams; where they intercept (gray area) is the most likely composition of the first meter below the surface of the Huygens landing site. This derivation was done assuming that the subsurface pores are saturated by liquid methane (Figure A.6a), filled with 50% of liquid methane (Figure A.6b) and empty (Figure A.6c). Constraints from microwave observations are obtained assuming a dielectric constant of 2.2 ± 0.1 (see section 4.1). Note that our approach requires a good estimate of the dielectric constant of the HLS which is not avail-

able to date, especially in the microwave domain. However, our goal here is to show that, if both the microwave and ELF dielectric constants of the ground were known with a good accuracy, we would be able to reliably constrain its composition because the constraints associated with these measurements are "perpendicular" to each other. This method could prove to be very valuable to future surface investigations of Titan.

While not very constraining, some lessons can be extracted from these diagrams. In particular, it seems that some porosity (at least 15%) and the presence of the water ice (at least 8%) are absolutely required to explain Cassini-Huygens observations while that of tholins is not. This means that the subsurface of the HLS could, in theory, consists of a porous water ice layer (60-75% water ice and 25-40% porosity if the pores are empty). However, the composition is most likely a combination of water ice and organic dust with some porosity, as suggested by the images taken at the surface by the Huygens probe and most of the plausible combinations displayed on Figure A.6. If the nature of the dust is tholin-like then its volumetric fraction in the first meter below the surface is at most 50-60%. Coherently, when the occupancy rate of the pores by liquid methane increases, less water ice and/or tholins are required in the mixture. The porosity should vary in the range 15-40% for empty pores and 30-65% for saturated pores.

4.3 Constraints on the composition of the HLS from the 11-min event

This work also offers the opportunity to investigate further the implications of our favorite scenario for the sudden drop of conductivity (or ϵ_r'') observed by the PWA-MIP/HASI instrument about 11 min after the Huygens landing [*Hamelin et al.*, 2016] (see also Table 2).

4.3.1 Description of observations

The conductivity drop observed by PWA-MIP/HASI occurred in a very short amount of time (2-4 s) and concerns an area, below the Huygens lander, as wide as the distance between the MIP electrodes i.e. 1-2 m [*Hamelin et al.*, 2016]. We reiterate that the concurrent observed decrease in ϵ_r' is not strong enough (relative to measurement uncertainty) to be considered significant. On the other hand, the HASI temperature sensors on board the Huygens probe did measure a significant drop of 0.2 K at the same time[*Hamelin et al.*, 2016] and the Huygens GCMS (Gas Chromatographer Mass Spectrometer) recorded a continuous increase in the atmospheric methane suggesting the progressive vaporization of methane in the subsurface due to heating by the probe [*Lorenz et al.*, 2006; *Niemann et al.*, 2010]. Additionally, the formation of a dewdrop was observed in a camera image and could be linked to rising air with high methane humidity also due to the heating of the surface by the bottom of the probe [*Karkoschka and Tomasko*, 2009]. Lastly, an unexplained attenuation was observed approximately 10 min after landing in the measurements performed by the acoustic instrument located near the bottom of the probe [*Lorenz et al.*, 2014].

4.3.2 Favored scenario

Based on these observations and the fact that the initially measured value of ϵ_r'' (0.5 ± 0.3) is much higher than the values expected for water ice and tholins (see Table 1) we favor the following course of events:

1. The Huygens probe was internally heated by internal power dissipation by the primary batteries during the descent and on the surface (around 250 W, [*Lorenz*, 2006]).
2. After landing, part of the heat was dissipated in the atmosphere by convection, the remaining being dissipated in the ground by conduction with the total heat dissipated being around 350 W [*Lorenz*, 2006].

3. This heating leads to the vaporization of a portion of the subsurface liquid hydrocarbons filling the pores.
4. An outgassing burst occurred about 11 min after landing and removed a thin superficial layer of dust responsible for the observed conductivity.

The vaporization of liquid hydrocarbons and, above all, the removal of a superficial conductive dust layer would explain the observed drop in the near-surface electrical properties. Such removal would affect mainly the imaginary part of the subsurface permittivity, as observed. We note that the final value measured by PWA-MIP/HASI (ϵ_r'' in the interval $0-0.1$) is compatible with a subsurface composed of any combination of water ice, tholins and vacuum.

As a further argument [*Lorenz*, 2006] estimates that a total of 500 kJ of energy could have been transferred to the subsurface in about an hour after landing. This would be sufficient to evaporate approximately 1 cm of liquid methane (approximately 0.91 kg). This value reduces to 0.2 kg if we take into account the possibility that the probe bounced before finding its final resting position (as suggested by *Schröder et al.* [2012]) reducing its contact with the surface (we consider a contact area 4 times smaller than *Lorenz* [2006]). Of importance, the penetrometer on board the Surface Science Package (SSP) of the Huygens probe detected the presence of a 7-mm dust layer at the landing site [*Atkinson et al.*, 2010]. This layer is likely composed of organic particles of low-density, therefore easily removable by the vaporizing of subsurface liquid.

4.3.3 Source of the conductivity

In the scenario previously mentioned the source of the conductivity is a thin layer of dust located at the surface and the removal of this layer would cause the observed drop in conductivity. Although solar UV can cause photoelectron production at planetary surfaces, in the case of Titan the UV flux is completely absorbed by the atmosphere and so this effect cannot influence the near-surface environment. Another possibility is the ionization of the near-surface atmosphere by decay of ^{14}C. According to [*Lorenz et al.*, 2002] the decay rate near the surface is capable of producing $10^4 \mathrm{cm}^{-2}$ ion pairs leading to a high air conductivity possibly detectable by PWA-MIP/Huygens. The outgassing from the subsurface could have led to the removal of the radiocarbons close to the probe therefore reducing the atmospheric conductivity in the vicinity of the instrument. This scenario could be modeled in order to evaluate the maximum conductivity of the atmosphere close to the lander and to appraise whether or not the atmospheric conductivity could explain the conductivity measured by PWA-MIP/HASI. However, the accurate modeling of this phenomenon and the addition of a highly conductive atmosphere near the Huygens probe is not a simple task and out of the scope of this work. In addition, we consider this scenario unlikely compared to the one described below.

Our favored explanation for the measured conductivity at the HLS after landing is the existence of a superficial layer of dust material with a non negligible intrinsic conductivity. In order to constrain the required characteristics, namely the thickness and conductivity, of this putative superficial conductive layer, we conducted numerical simulations with a finite element code (COMSOL Multiphysics™, see [*Hamelin et al.*, 2016] for more detail) assuming a 2-layer subsurface. The numerical simulations take in account the whole of the Huygens probe (for numerical reasons the probe's shape had to be simplified, see [*Hamelin et al.*, 2016] for the details of the simplification) in its two extreme attitudes at the surface (see [*Hamelin et al.*, 2016] for a description of these extreme cases). Performing numerical simulations for a set of thicknesses of the dust layer we provide estimates of the dust electrical conductivity required to explain the observed drop in electrical conductivity 11 min after landing. Figure A.7 shows the resulting upper and lower limits of the imaginary part of the effective permittivity of the conductive layer as a function of its thickness (the upper and lower limits include the uncertainty on the probe attitude at

the surface, whereas the error bars account for the numerical error of the model and the measurement uncertainty of the PWA-MIP/HASI instrument). We note that if the thickness of the removed conductive layer is 7 mm (as suggested by [*Atkinson et al.*, 2010]) then the imaginary part of its permittivity must be relatively high, namely between 2.8 and 16.0 (corresponding to a conductivity in the range 7-40 nS/m). Logically, the required imaginary part of the permittivity decreases as the thickness of the conductive layer increases; its lower limit is 0.5 ± 0.3.

4.3.4 Composition of the dust layer

Regarding the implications of this investigation on the composition of the putative conductive 7 mm superficial layer, we are unfortunately hampered by the lack of available information in literature on the conductivity of materials relevant to Titan's at low temperatures and low frequencies. One thing is certain: the tholins studied in this work do not have a high enough imaginary part to be a major component of this layer. Likewise, the DC conductivity of polyacetylene at 200 K is at most 10^{-7} S/m^{-1} and shows a linear decrease with temperature [*Jones et al.*, 1991], preventing it from being a major component of this layer. On the other hand, some polymers, such as polyaniline, or in general, nitrile-rich organic compounds may be more conductive but their accurate electrical properties remain unknown [*Le Gall et al.*, 2016]. Also, nanophase iron and nanophase hematite which are present in Saturn's rings and on the surface of Iapetus [*Clark et al.*, 2012] may have relatively high conductivity at low frequencies/low temperatures: *Nikolic et al.* [2012] measured the DC electrical conductivity of hematite doped with Zn and, by extrapolating their results at Titan's surface temperature, the maximum conductivity is found to 10^{-8} S/m, therefore, the possibility that hematite (doped with 10% Zn) as a major component of this layer cannot be excluded but is very low (the highest conductivity value of this component is only slightly higher than the lowest possible conductivity of this layer, additionally, this only applies to hematite with high Zn content, higher than 10%). Although no measurement of electrical properties of nanophase iron relevant to Titan were found in the literature, powdered metals tend to have a high conductivity. Therefore nanophase iron is most likely at least somewhat conductive and could be a potential component of this layer. Lastly, we note that the photochemical aging of Titan's aerosols during their sedimentation through Titan's atmosphere [*Couturier-Tamburelli et al.*, 2018] and possibly also at the surface can produce aerosols that are more conductive that the "fresh" tholins synthesized in laboratory and analyzed in this work. Future works should consider investigating the electrical properties of "processed tholins".

5 Conclusion and perspectives

The measurements performed by the PWA-MIP/HASI/Huygens/Cassini-Huygens instrument in 2005 provided unique insights into the electrical properties of the first meter of Titan's subsurface. However, in order to convert these measurements in term of composition, the low-frequency and low temperature electrical properties of materials possibly present at the surface of Titan need to be known. In this paper, we present the first low frequency electrical characterization of samples of tholins. Tholins are organic matter, possibly analogous to the aerosols produced in the atmosphere of Titan and then deposited onto the surface. Their electrical characterization was performed with a dedicated measurement bench developed at LATMOS. We find that the electrical properties of tholins follow predictable variations (i.e., the real and imaginary parts of the permittivity decrease with higher frequency, higher porosity and lower temperature) and show significant variations as a function of the composition of the gaseous mixture from which they were produced. Based on multi-frequency laboratory electrical characterizations and combining measurements from PWA-MIP/HASI and the Cassini Radar, we derive constraints on the composition of the Huygens Landing Site. While not very strong (a porosity between 15%

and 65%, a maximum of 60% of tholins and between 20% and 75% of water ice) our results and approach can serve as a frame of reference for future studies.

We also expand the study of the sudden and significant drop of conductivity observed about 11 min after the landing of Huygens at the surface of Titan which was presented in *Hamelin et al.* [2016]. Our favored scenario describes how the subsurface was heated by the probe after landing enough for some subsurface methane to vaporize . This vaporizing methane may have then depleted a thin superficial conductive dust layer. Based on this scenario and numerical simulations we estimate the imaginary part of this conductive dust layer to be at least 2.8 which is very high and rules out the tholins we studied as a main component of the putative superficial dust layer. To our knowledge there is no material relevant to Titan's surface composition with such a high conductivity (more precisely, the only known possibility would be hematite with a high quantity of Zn). However, the electrical properties of a great number of possible materials remain to be investigated and we therefore emphasize the need for more laboratory characterization over wide range of frequencies.

Lastly, we note that this work and our analysis approach will be useful for future missions to Titan and, in particular, missions including a permittivity probe such as the Dragonfly mission [*Turtle et al.*, 2017], a relocatable quadcopter recently pre-selected for the New Frontiers program. If the mission is selected, Dragonfly permittivity measurements will most likely be more accurate than those performed by PWA-MIP/HASI and will therefore provide much stronger constraints on the plausible composition of Titan's subsurface and even discriminate between the different types of tholins at the surface . We also note for future missions to Titan, that, in order to differentiate between the different composition of tholins based on their electrical properties, certain frequencies would be more useful than others. More specifically, at Titan's surface temperature, while the real part shows significant difference between compositions at all frequencies (see Figure 5 left), the most relevant frequencies to capture differences in the imaginary part due to composition are 100, 1000 and 5000 Hz (see Figure A.4a.).

A: Measurements and derivation of the sample complex permittivity

The spectrum analyzer measures the complex impedance of the sample between the electrodes sweeping the frequency range 1 Hz-100 kHz. For a given frequency, the same measurement is repeated 3 times and the average value is recorded. It takes about 22 s to measure the complex impedance over a full frequency spectrum. At the end of a typical measurement cycle which lasts about 20 h (10h for the liquid nitrogen to evaporate and 10 hours for the sample to return to room temperature), 3000 to 4000 spectra have been collected.

The measured complex impedance Z_s (in Ω) is related to the capacitance C (in F) of the parallel plate electrodes by:

$$C_s = \frac{1}{2\pi f j Z_s} \tag{A.1}$$

where f is the frequency of the input signal.

The complex capacitance of a parallel-plate capacitor is itself related to the complex relative permittivity of the medium between the parallel electrodes by:

$$\epsilon_r = \frac{C_s d}{A\epsilon_0} \tag{A.2}$$

where A [m^2] is the surface area of the electrodes (and generally of the sample) and d [m] is the thickness of the sample.

Equation A.2 applies well if the distance between the electrodes remains much smaller than their dimensions. In addition, it assumes that the electrical field is entirely concentrated in the dielectric medium between the plates and thus neglects edge effects which induce parasitic capacitances.

In order to correct measurements performed on samples from parasitic effects, we calibrate them by measurements made with an empty cell i.e., measurements performed after removing the sample from the sample holder but without changing the distance d between the electrodes. More specifically, we measure Z_{void} and thus C_{void} and equation A.2 becomes:

$$\epsilon_r = \frac{C_c d}{A \epsilon_0} \tag{A.3}$$

with C_c the corrected complex capacitance:

$$C_c = C_s + \frac{\epsilon_0 A}{d} - C_{void} \tag{A.4}$$

The effects of the electronics were evaluated and found to be negligible.

Acknowledgments

The PAP measurement bench was partialy funded by the DIM-ACAV (Domaine d'Intêret Majeur-Astrophysique et Conditions d'Apparition de la Vie) program of the Région Ile-de-France. The CNES (Centre National d'Etude Spatiale) also provided financial help for material resources. The data reported in this paper are freely available at: `ftp:/ftp.latmos.ipsl.fr/outgoing/lethuillier/PAP_data/`. The authors would like to thank Ralph Lorenz and Elizabeth Turtle for their valuable comments from which the paper greatly benefited.

References

Atkinson, K. R., J. C. Zarnecki, M. C. Towner, T. J. Ringrose, A. Hagermann, A. J. Ball, M. R. Leese, G. Kargl, M. D. Paton, R. D. Lorenz, and S. F. Green (2010), Penetrometry of granular and moist planetary surface materials: Application to the Huygens landing site on Titan, *Icarus*, *210*, 843–851, doi:10.1016/j.icarus.2010.07.019.

Barnes, J. W., R. H. Brown, L. Soderblom, C. Sotin, S. L. Mouèlic, S. Rodriguez, R. Jaumann, R. A. Beyer, B. J. Buratti, K. Pitman, K. H. Baines, R. Clark, and P. Nicholson (2008), Spectroscopy, morphometry, and photoclinometry of titan's dunefields from cassini/vims, *Icarus*, *195*(1), 400 – 414, doi:https://doi.org/10.1016/j.icarus.2007.12.006.

Borucki, W. J., Z. Levin, R. C. Whitten, R. G. Keesee, L. A. Capone, A. L. Summers, O. B. Toon, and J. Dubach (1987), Predictions of the electrical conductivity and charging of the aerosols in Titan's atmosphere, *Icarus*, *72*, 604–622, doi:10.1016/0019-1035(87)90056-X.

Brouet, Y., A. C. Levasseur-Regourd, P. Sabouroux, L. Neves, P. Encrenaz, O. Poch, A. Pommerol, N. Thomas, W. Kofman, A. Le Gall, V. Ciarletti, A. Hérique, A. Lethuillier, N. Carrasco, and C. Szopa (2016), A porosity gradient in 67p/C-G nucleus suggested from CONSERT and SESAME-PP results: an interpretation based on new laboratory permittivity measurements of porous icy analogues, *Monthly Notices of the Royal Astronomical Society*, *462*, S89–S98, doi:10.1093/mnras/stw2151.

Cable, M. L., S. M. Hörst, R. Hodyss, P. M. Beauchamp, M. A. Smith, and P. A. Willis (2012), Titan Tholins: Simulating Titan Organic Chemistry in the Cassini-Huygens Era, *Chemical Reviews*, *112*, 1882–1909, doi:10.1021/cr200221x.

Campbell, D. B., G. J. Black, L. M. Carter, and S. J. Ostro (2003), Radar Evidence for Liquid Surfaces on Titan, *Science*, *302*, 431–434, doi:10.1126/science.1088969.

Carrasco, N., T. Gautier, E.-t. Es-sebbar, P. Pernot, and G. Cernogora (2012), Volatile products controlling Titan's tholins production, *Icarus*, *219*, 230–240, doi:10.1016/j.icarus.2012.02.034.

Clark, S. P. (1966), *Handbook of Physical Constants*, Geological Society of America.

Clark, R. N., J. M. Curchin, J. W. Barnes, R. Jaumann, L. Soderblom, D. P. Cruikshank, R. H. Brown, S. Rodriguez, J. Lunine, K. Stephan, T. M. Hoefen, S. Le Mouélic, C. Sotin, K. H. Baines, B. J. Buratti, and P. D. Nicholson (2010), Detection and mapping of hydrocarbon deposits on Titan, *Journal of Geophysical Research: Planets*, *115*, E10,005, doi:10.1029/2009JE003369.

Clark, R. N., D. P. Cruikshank, R. Jaumann, R. H. Brown, K. Stephan, C. M. D. Ore, K. E. Livo, N. Pearson, J. M. Curchin, T. M. Hoefen, B. J. Buratti, G. Filacchione, K. H. Baines, and P. D. Nicholson (2012), The surface composition of iapetus: Mapping results from cassini vims, *Icarus*, *218*(2), 831 – 860, doi:https://doi.org/10.1016/j.icarus.2012.01.008.

Clausen, K. C., H. Hassan, M. Verdant, P. Couzin, G. Huttin, M. Brisson, C. Sollazzo, and J.-P. Lebreton (2002), The Huygens Probe System Design, *Space Science Reviews*, *104*, 155–189, doi:10.1023/A:1023648925732.

Cole, K. S., and R. H. Cole (1941), Dispersion and Absorption in Dielectrics I. Alternating Current Characteristics, *The Journal of Chemical Physics*, *9*, 341–351, doi:10.1063/1.1750906.

Couturier-Tamburelli, I., N. Piétri, V. Le Letty, T. Chiavassa, and M. Gudipati (2018), UV–Vis Light-induced Aging of Titan's Haze and Ice, *The Astrophysical Journal*, *852*(2), 117, doi:https://doi.org/10.3847/1538-4357/aa9e8d.

Derenne, S., C. Coelho, C. Anquetil, C. Szopa, A. Rahman, P. McMillan, F. Corà, C. Pickard, E. Quirico, and C. Bonhomme (2012), New insights into the structure and chemistry of titan's tholins via 13c and 15n solid state nuclear magnetic resonance spectroscopy, *Icarus*, *221*(2), 844 – 853, doi:https://doi.org/10.1016/j.icarus.2012.03.003.

Elachi, C., M. D. Allison, L. Borgarelli, P. Encrenaz, E. Im, M. A. Janssen, W. T. K. Johnson, R. L. Kirk, R. D. Lorenz, J. I. Lunine, D. O. Muhleman, S. J. Ostro, G. Picardi, F. Posa, C. G. Rapley, L. E. Roth, R. Seu, L. A. Soderblom, S. Vetrella, S. D. Wall, C. A. Wood, and H. A. Zebker (2004), Radar: The cassini titan radar mapper, *Space Science Reviews*, *115*(1), 71–110, doi:10.1007/s11214-004-1438-9.

Feuerbacher, B., M. Anderegg, B. Fitton, L. D. Laude, R. F. Willis, and R. J. L. Grard (1972), Photoemission from lunar surface fines and the lunar photoelectron sheath, in *Lunar and Planetary Science Conference Proceedings*, *Lunar and Planetary Science Conference Proceedings*, vol. 3, edited by A. E. Metzger, J. I. Trombka, L. E. Peterson, R. C. Reedy, and J. R. Arnold, p. 2655.

Fulchignoni, M., F. Ferri, F. Angrilli, A. J. Ball, A. Bar-Nun, M. A. Barucci, C. Bettanini, G. Bianchini, W. Borucki, G. Colombatti, M. Coradini, A. Coustenis, S. Debei, P. Falkner, G. Fanti, E. Flamini, V. Gaborit, R. Grard, M. Hamelin, A. M. Harri, B. Hathi, I. Jernej, M. R. Leese, A. Lehto, P. F. Lion Stoppato, J. J. Lopez-Moreno, T. Makinen, J. A. M. McDonnell, C. P. McKay, G. Molina-Cuberos, F. M. Neubauer, V. Pirronello, R. Rodrigo, B. Saggin, K. Schwingenschuh, A. Seiff, F. Simoes, H. Svedhem, T. Tokano, M. C. Towner, R. Trautner, P. Withers, and J. C. Zarnecki (2005), In situ measurements of the physical characteristics of Titan's environment, *Nature*, *438*, 785–791, doi:10.1038/nature04314.

Garnett, J. C. M. (1904), Colours in Metal Glasses and in Metallic Films, *Philosophical Transactions of the Royal Society of London A: Mathematical, Physical and Engineering Sciences*, *203*, 385–420, doi:10.1098/rsta.1904.0024.

Grard, R. (1995), Solar photon interaction with the martian surface and related electrical and chemical phenomena, *Icarus*, *114*(1), 130 – 138, doi:https://doi.org/10.1006/icar.1995.1048.

Grard, R., M. Hamelin, J. J. López-Moreno, K. Schwingenschuh, I. Jernej, G. J. Molina-Cuberos, F. Simões, R. Trautner, P. Falkner, F. Ferri, M. Fulchignoni, R. Rodrigo, H. Svedhem, C. Béghin, J. J. Berthelier, V. J. G. Brown, M. Chabassière, J. M. Jeronimo, L. M. Lara, and T. Tokano (2006), Electric properties and related physical characteristics of the atmosphere and surface of Titan, *Planetary and Space Science*, *54*, 1124–1136, doi:10.1016/j.pss.2006.05.036.

Griffith, C. A., T. Owen, T. R. Geballe, J. Rayner, and P. Rannou (2003), Evidence for the Exposure of Water Ice on Titan's Surface, *Science*, *300*, 628–630, doi:10.1126/science.1081897.

Grundy, W. M., R. P. Binzel, B. J. Buratti, J. C. Cook, D. P. Cruikshank, C. M. D. Ore, A. M. Earle, K. Ennico, C. J. A. Howett, A. W. Lunsford, C. B. Olkin, A. H. Parker, S. Philippe, S. Protopapa, E. Quirico, D. C. Reuter, B. Schmitt, K. N. Singer, A. J. Verbiscer, R. A. Beyer, M. W. Buie, A. F. Cheng, D. E. Jennings, I. R. Linscott, J. W. Parker, P. M. Schenk, J. R. Spencer, J. A. Stansberry, S. A. Stern, H. B. Throop, C. C. C. Tsang, H. A. Weaver, G. E. Weigle, L. A. Young, and a. t. N. H. S. Team (2016), Surface compositions across Pluto and Charon, *Science*, *351*, 6279, doi:10.1126/science.aad9189.

Hadamcik, E., J. B. Renard, G. Alcouffe, G. Cernogora, A. C. Levasseur-Regourd, and C. Szopa (2009), Laboratory light-scattering measurements with Titan's aerosols analogues produced by a dusty plasma, *Planetary and Space Science*, *57*, 1631–1641, doi:10.1016/j.pss.2009.06.013.

Hamelin, M., A. Lethuillier, A. Le Gall, R. Grard, C. Béghin, K. Schwingenschuh, I. Jernej, J.-J. López-Moreno, V. Brown, R. D. Lorenz, F. Ferri, and V. Ciarletti (2016), The electrical properties of Titan's surface at the Huygens landing site measured with the PWA–HASI Mutual Impedance Probe. New approach and new findings, *Icarus*, *270*, 272–290, doi:10.1016/j.icarus.2015.11.035.

Hashin, Z., and S. Shtrikman (1962), A variational approach to the theory of the effective magnetic permeability of multiphase materials, *Journal of Applied Physics*, *33*, 3125–3131, doi:10.1063/1.1728579.

Hestermans, P., and D. White (1961), The vapor pressures, heats of vaporization and heat capacities of methane from the boiling point to the critical temperature., *The Journal of Physical Chemistry*, *65*, 362–365, doi:10.1021/j100820a044.

Hörst, S. M., and M. A. Tolbert (2013), In situ measurements of the size and density of titan aerosol analogs, *The Astrophysical Journal Letters*, *770*(1), L10.

Imanaka, H., D. P. Cruikshank, B. N. Khare, and C. P. McKay (2012), Optical constants of titan tholins at mid-infrared wavelengths (2.5–25μm) and the possible chemical nature of titan's haze particles, *Icarus*, *218*(1), 247 – 261, doi:https://doi.org/10.1016/j.icarus.2011.11.018.

Janssen, M. A., R. D. Lorenz, R. West, F. Paganelli, R. M. Lopes, R. L. Kirk, C. Elachi, S. D. Wall, W. T. K. Johnson, Y. Anderson, R. A. Boehmer, P. Callahan, Y. Gim, G. A. Hamilton, K. D. Kelleher, L. Roth, B. Stiles, and A. Le Gall (2009), Titan's surface at 2.2-cm wavelength imaged by the Cassini RADAR radiometer: Calibration and first results, *Icarus*, *200*, 222–239, doi:10.1016/j.icarus.2008.10.017.

Janssen, M. A., A. Le Gall, R. M. Lopes, R. D. Lorenz, M. J. Malaska, A. G. Hayes, C. D. Neish, A. Solomonidou, K. L. Mitchell, J. Radebaugh, S. J. Keihm, M. Choukroun, C. Leyrat, P. J. Encrenaz, and M. Mastrogiuseppe (2016), Titan's surface at 2.18-cm wavelength imaged by the Cassini RADAR radiometer: Results and interpretations through the first ten years of observation, *Icarus*, *270*, 443–459, doi:10.1016/j.icarus.2015.09.027.

Jones, C., R. Lawrence, J. Martens, R. Friend, D. Parker, W. Feast, M. Lögdlund, and W. Salaneck (1991), Electronic properties of polyacetylene prepared by the

durham ‘photoisomer’ route, *Polymer*, *32*(7), 1200 – 1209, doi:https://doi.org/10.1016/0032-3861(91)90222-5.

Karkoschka, E., M. G. Tomasko, L. R. Doose, C. See, E. A. McFarlane, S. E. Schröder, and B. Rizk (2007), DISR imaging and the geometry of the descent of the Huygens probe within Titan’s atmosphere, *Planetary and Space Science*, *55*, 1896–1935, doi:10.1016/j.pss.2007.04.019.

Karkoschka, E., and M. G. Tomasko (2009), Rain and dewdrops on titan based on in situ imaging, *Icarus*, *199*(2), 442 – 448, doi:https://doi.org/10.1016/j.icarus.2008.09.020.

Gall, A. L., M. Janssen, L. Wye, A. Hayes, J. Radebaugh, C. Savage, H. Zebker, R. Lorenz, J. Lunine, R. Kirk, R. Lopes, S. Wall, P. Callahan, E. Stofan, and T. Farr (2011), Cassini sar, radiometry, scatterometry and altimetry observations of titan’s dune fields, *Icarus*, *213*(2), 608 – 624, doi:https://doi.org/10.1016/j.icarus.2011.03.026.

Le Gall, A., M. J. Malaska, R. D. Lorenz, M. A. Janssen, T. Tokano, A. G. Hayes, M. Mastrogiuseppe, J. I. Lunine, G. Veyssière, P. Encrenaz, and O. Karatekin (2016), Composition, seasonal change, and bathymetry of Ligeia Mare, Titan, derived from its microwave thermal emission, *Journal of Geophysical Research: Planets*, *121*,233–251,doi:10.1002/2015JE004920.

Lebreton, J.-P., and D. L. Matson (2004), The Huygens mission to Titan: an overview, in *Titan - From Discovery to Encounter*, *ESA Special Publication*, vol. 1278, edited by K. Fletcher, pp. 229–242.

Lebreton, J.-P., O. Witasse, C. Sollazzo, T. Blancquaert, P. Couzin, A.-M. Schipper, J. B. Jones, D. L. Matson, L. I. Gurvits, D. H. Atkinson, B. Kazeminejad, and M. Pérez-Ayúcar (2005), An overview of the descent and landing of the Huygens probe on Titan, *Nature*, *438*, 758–764, doi:10.1038/nature04347.

Leese, M. R., R. D. Lorenz, B. Hathi, and J. C. Zarnecki (2012), The Huygens surface science package (SSP): Flight performance review and lessons learned, *Planetary and Space Science*, *70*, 28–45, doi:10.1016/j.pss.2012.06.005.

Lethuillier, A. (2016), Characterization of planetary subsurfaces with permittivity probes : analysis of the SESAME-PP/Philae and PWA-MIP/HASI/Huygens data, Theses, Université Paris-Saclay.

Rodriguez, S., P. Paillou, M. Dobrijevic, G. Ruffié, P. Coll, J. M. Bernard, and P. Encrenaz (2003), Impact of aerosols present in Titan’s atmosphere on the CASSINI radar experiment, *Icarus*, *164*, 213–227, doi:10.1016/S0019-1035(03)00125-8.

Lopes, R., E. Stofan, R. Peckyno, J. Radebaugh, K. Mitchell, G. Mitri, C. Wood, R. Kirk, S. Wall, J. Lunine, A. Hayes, R. Lorenz, T. Farr, L. Wye, J. Craig, R. Ollerenshaw, M. Janssen, A. LeGall, F. Paganelli, R. West, B. Stiles, P. Callahan, Y. Anderson, P. Valora, and L. Soderblom (2010), Distribution and interplay of geologic processes on titan from cassini radar data, *Icarus*, *205*(2), 540 – 558, doi:https://doi.org/10.1016/j.icarus.2009.08.010.

Lorenz, R., and J. Mitton (2002), *Lifting Titan’s Veil: Exploring the Giant Moon of Saturn*, Cambridge University Press.

Lorenz, R., A. Jull, T. Swindle, and J. I. Lunine (2002), Radiocarbon on titan, *Meteoritics & Planetary Science*, *37*, 867 – 874.

Lorenz, R. D. (2006), Thermal interactions of the huygens probe with the titan environment: Constraint on near-surface wind, *Icarus*, *182*(2), 559 – 566, doi:https://doi.org/10.1016/j.icarus.2006.01.009

Lorenz, R. D., H. B. Niemann, D. N. Harpold, S. H. Way, and J. C. Zarnecki (2006), Titan’s damp ground: Constraints on titan surface thermal properties from the temperature evolution of the huygens gcms inlet, *Meteoritics and Planetary Science*, *41*(11), 1705–1714, doi:10.1111/j.1945-5100.2006.tb00446.x.

Lorenz, R. D., M. R. Leese, B. Hathi, J. C. Zarnecki, A. Hagermann, P. Rosenberg, M. C. Towner, J. Garry, and H. Svedhem (2014), Silence on shangri-la: Attenuation of huygens acoustic signals suggests surface volatiles, *Planetary and Space Science*, *90*(Supplement C), 72 – 80, doi:https://doi.org/10.1016/j.pss.2013.11.003.

Lorenz, R. D. (2014), The flushing of Ligeia: Composition variations across Titan's seas in a simple hydrological model, *Geophysical Research Letters*, *41*, 5764–5770, doi:10.1002/2014GL061133.

Mahjoub, A., N. Carrasco, P.-R. Dahoo, T. Gautier, C. Szopa, and G. Cernogora (2012), Influence of methane concentration on the optical indices of titan's aerosols analogues, *Icarus*, *221*(2), 670 – 677, doi:https://doi.org/10.1016/j.icarus.2012.08.015.

Mahjoub, A., M. Schwell, N. Carrasco, Y. Benilan, G. Cernogora, C. Szopa, and M.-C. Gazeau (2016), Characterization of aromaticity in analogues of titan's atmospheric aerosols with two-step laser desorption ionization mass spectrometry, *Planetary and Space Science*, *131*(Supplement C), 1 – 13, doi:https://doi.org/10.1016/j.pss.2016.05.003.

Mattei, E., S. E. Lauro, G. Vannaroni, B. Cosciotti, F. Bella, and E. Pettinelli (2014), Dielectric measurements and radar attenuation estimation of ice/basalt sand mixtures as martian Polar Caps analogues, *Icarus*, *229*, 428–433, doi:10.1016/j.icarus.2013.10.017.

McDonald, G. D., W. R. Thompson, M. Heinrich, B. N. Khare, and C. Sagan (1994), Chemical Investigation of Titan and Triton Tholins, *Icarus*, *108*, 137–145, doi:10.1006/icar.1994.1046.

McDonald, G. D., L. J. Whited, C. DeRuiter, B. N. Khare, A. Patnaik, and C. Sagan (1996), Production and Chemical Analysis of Cometary Ice Tholins, *Icarus*, *122*, 107–117, doi:10.1006/icar.1996.0112.

Mishra, A., M. Michael, S. N. Tripathi, and C. Béghin (2014), Revisited modeling of Titan's middle atmosphere electrical conductivity, *Icarus*, *238*, 230–234, doi:10.1016/j.icarus.2014.04.018.

Mitchell, K. L., M. B. Barmatz, C. S. Jamieson, R. D. Lorenz, and J. I. Lunine (2015), Laboratory measurements of cryogenic liquid alkane microwave absorptivity and implications for the composition of Ligeia Mare, Titan, *Geophysical Research Letters*, *42*, 1340–1345, doi:10.1002/2014GL059475.

Niemann, H. B., S. K. Atreya, J. E. Demick, D. Gautier, J. A. Haberman, D. N. Harpold, W. T. Kasprzak, J. I. Lunine, T. C. Owen, and F. Raulin (2010), Composition of Titan's lower atmosphere and simple surface volatiles as measured by the Cassini-Huygens probe gas chromatograph mass spectrometer experiment, *Journal of Geophysical Research: Planets*, *115*, E12006, doi:10.1029/2010JE003659.

Nikolic, M., M. Slankamenac, N. Nikolic, D. Sekulic, O. Aleksic, M. Mitric, T. Ivetic, V. Pavlovic, and P. Nikolic (2012), Study of dielectric behavior and electrical properties of hematite a-fe 2 o 3 doped with zn, *Science of Sintering*, *44*, 307.

Paillou, P., J. Lunine, G. Ruffié, P. Encrenaz, S. Wall, R. Lorenz, and M. Janssen (2008), Microwave dielectric constant of Titan-relevant materials, *Geophysical Research Letters*, *35*, L18202, doi:10.1029/2008GL035216.

Pettinelli, E., S. E. Lauro, B. Cosciotti, E. Mattei, F. D. Paolo, and G. Vannaroni (2016), Dielectric characterization of ice/mgso4·11h2o mixtures as jovian icy moon crust analogues, *Earth and Planetary Science Letters*, *439*(Supplement C), 11 – 17, doi:https://doi.org/10.1016/j.epsl.2016.01.021.

Sagan, C., and B. Khare (1979), Tholins: Organic chemistry of interstellar grains and gas, *Nature*, *279*, 102–107, doi:10.1038/277102a0.

Sagan, C., B. N. Khare, W. R. Thompson, G. D. McDonald, M. R. Wing, J. L. Bada, T. Vo-Dinh, and E. T. Arakawa (1993), Polycyclic aromatic hydrocarbons in the atmospheres of Titan and Jupiter, *The Astrophysical Journal*, *414*, 399–405.

Schröder, S. E., E. Karkoschka, and R. D. Lorenz (2012), Bouncing on Titan: Motion of the Huygens probe in the seconds after landing, *Planetary and Space Science*, *73*, 327–340, doi:10.1016/j.pss.2012.08.007.

Mastrogiuseppe, M., V. Poggiali, A. Hayes, R. Lorenz, J. Lunine, G. Picardi, R. Seu, E. Flamini, G. Mitri, C. Notarnicola, P. Paillou, and H. Zebker (2014), The bathymetry of a titan sea, *Geophysical Research Letters*, *41*(5), 1432–1437, doi:10.1002/2013GL058618, 2013GL058618.

Table A.1. Electrical properties of material relevant to Titan's surface at 94 K and at 2 frequencies, namely that of PWA-MIP/HASI and that of the Cassini Radar.

Frequencies	45 Hz		14 GHz	
	ϵ_r'	$\epsilon_r'' \times 10^{-2}$	ϵ_r'	$\epsilon_r'' \times 10^{-3}$
Tholins 2%	4.00 ± 0.04	1.05 ± 0.03	1.17 (non-compacted)[b] 2.33 (compacted)[b]	3.3 (non-compacted)[b] 20.6 (compacted)[b]
Tholins 5%	4.40 ± 0.05	1.68 ± 0.13	N/A	N/A
Tholins 8%	3.40 ± 0.04	1.37 ± 0.04	N/A	N/A
Water ice	3.15[a]	0.40[a]	3.13 ± 0.30[a]	1.30 ± 0.26[a]
Liquid methane	1.67[d]	N/A	1.74 ± 0.03[c]	(4.93 ± 2.50) × 10^{-2}[c]

[a] Extrapolated from *Mattei et al.* [2014], [b] [*Paillou et al.*, 2008]
[c] [*Mitchell et al.*, 2015] , [d] [*Leese et al.*, 2012] at 100 Hz.

Sciamma-O'Brien, E., N. Carrasco, C. Szopa, A. Buch, and G. Cernogora (2010), Titan's atmosphere: An optimal gas mixture for aerosol production?, *Icarus*, *209*, 704–714, doi: 10.1016/j.icarus.2010.04.009.

Simões, F., R. Trautner, R. Grard, and M. Hamelin (2004), Laboratory Measurements on Martian Soil Simulant JSC Mars-1 Supporting the Calibration of Instruments for Planetary Missions, in *Proceedings of the 37th ESLAB Symposium "Tools and Technologies for Future Planetary Exploration"*, vol. 543, pp. 205–209.

Stern, S. A., L. M. Feaga, E. Schindhelm, A. Steffl, J. W. Parker, P. D. Feldman, H. A. Weaver, M. F. A'Hearn, J. Cook, and J. L. Bertaux (2015), First extreme and far ultraviolet spectrum of a Comet Nucleus: Results from 67p/Churyumov-Gerasimenko, *Icarus*, *256*, 117–119, doi:10.1016/j.icarus.2015.04.023.

Szopa, C., G. Cernogora, L. Boufendi, J. J. Correia, and P. Coll (2006), PAMPRE: A dusty plasma experiment for Titan's tholins production and study, *Planetary and Space Science*, *54*, 394–404, doi:10.1016/j.pss.2005.12.012.

Tobie, G., O. Grasset, J. I. Lunine, A. Mocquet, and C. Sotin (2005), Titan's internal structure inferred from a coupled thermal-orbital model, *Icarus*, *175*, 496–502, doi: 10.1016/j.icarus.2004.12.007.

Trainer, M. G., A. A. Pavlov, H. L. DeWitt, J. L. Jimenez, C. P. McKay, O. B. Toon, and M. A. Tolbert (2006), Organic haze on titan and the early earth, *Proceedings of the National Academy of Sciences*, *103*(48), 18,035–18,042, doi:10.1073/pnas.0608561103.

Turtle, E. P., J. W. Barnes, M. G. Trainer, R. D. Lorenz, S. M. MacKenzie, K. E. Hibbard, D. Adams, P. Bedini, J. W. Langelaan, K. Zacny, and Dragonfly Team (2017), Dragonfly: Exploring Titan's Prebiotic Organic Chemistry and Habitability, in *Lunar and Planetary Science Conference*, *Lunar and Planetary Science Conference*, vol. 48, p. 1958.

Waite, J. H., D. T. Young, T. E. Cravens, A. J. Coates, F. J. Crary, B. Magee, and J. Westlake (2007), The Process of Tholin Formation in Titan's Upper Atmosphere, *Science*, *316*, 870–875, doi:10.1126/science.1139727.

Wye, L. C. (2011), Radar Scattering from Titan and Saturn's Icy Satellites Using the Cassini Spacecraft, Ph.D. thesis, Stanford University.

Wye, L. C., H. A. Zebker, S. J. Ostro, R. D. West, Y. Gim, R. D. Lorenz, and the Cassini RADAR Team (2007), Electrical properties of Titan's surface from Cassini RADAR scatterometer measurements, *Icarus*, *188*, 367–385, doi:10.1016/j.icarus.2006.12.008.

Zarnecki, J. C., M. R. Leese, B. Hathi, A. J. Ball, A. Hagermann, M. C. Towner, R. D. Lorenz, J. A. M. McDonnell, S. F. Green, M. R. Patel, T. J. Ringrose, P. D. Rosenberg, K. R. Atkinson, M. D. Paton, M. Banaszkiewicz, B. C. Clark, F. Ferri, M. Fulchignoni, N. A. L. Ghafoor, G. Kargl, H. Svedhem, J. Delderfield, M. Grande, D. J. Parker, P. G. Challenor, and J. E. Geake (2005), A soft solid surface on Titan as revealed by the Huygens Surface Science Package, *Nature*, *438*, 792–795, doi:10.1038/nature04211.

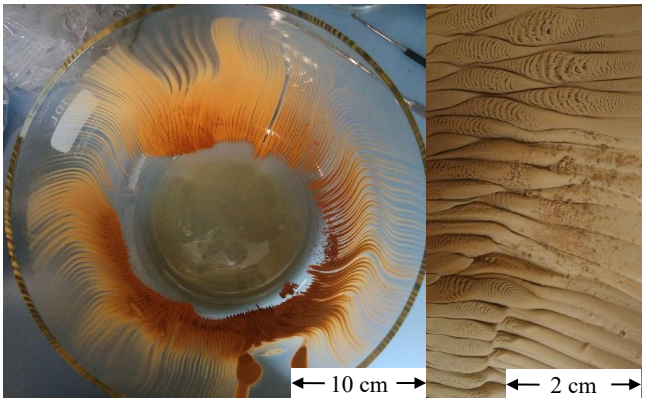

892 **Figure A.1.** Tholins produced by the PAMPRE experiment with a gas mixture of 92/8 ratio of N2/CH4.

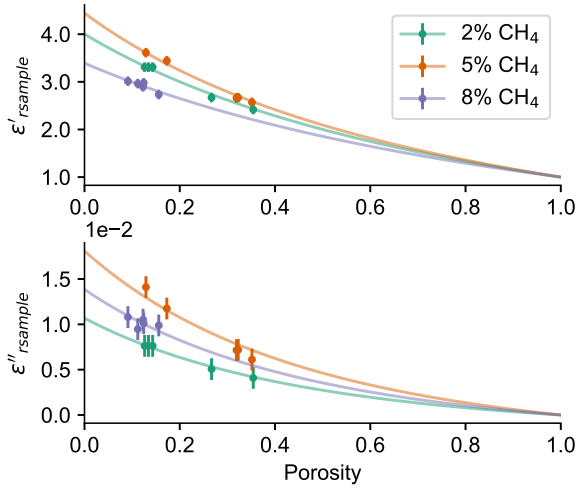

895 **Figure A.2.** Real (top) and imaginary (bottom) parts of the complex permittivity of tholins as a function of
896 the porosity of the samples measured for three different compositions. The data points are for a temperature of
897 94 K and a frequency f = 100 Hz. The continuous lines represent the Maxwell-Garnett mixing law.

Table A.2. Remote sensing (from the Earth and the Cassini spacecraft) and in-situ (with the Huygens probe) measurements of the electrical properties of the first meters of Titan's subsurface.

Instrument	Frequency (wavelength)	Region	ϵ_r'	ϵ_r''	Reference
Arecibo Radar System	2.4 GHz (13 cm)	Latitude band at 26°S	1.5-2.2 with a mean value of 1.8 ± 0.3	N/A	[*Campbell et al.*, 2003]
Cassini Radar Scatterometer	13.8 GHz (2.2 cm)	Average over globe	2.12 ± 0.07	N/A	[*Wye et al.*, 2007]
		Plains (HLS-like?)	1.9-3.6 with a mean value of 2.2 ± 0.05	N/A	[*Wye*, 2011]
Cassini Radar Radiometer Polarized	13.8 GHz (2.2 cm)	Average over globe	1.54	N/A	[*Janssen et al.*, 2016]
		HLS region	1.7 ± 0.2	N/A	
Cassini Radar Radiometer Emissivity	13.8 GHz (2.2 cm)	HLS region	2.7 ± 0.25	$\approx 10^{-3}$	[*Janssen et al.*, 2016]
PWA-MIP/HASI	45 Hz	HLS	2.55 ± 0.35 (<11 min) 2.35 ± 0.35 (>11 min)	$0.2 - 0.8$ (<11 min) $0 - 0.1$ (>11 min)	[*Hamelin et al.*, 2016]

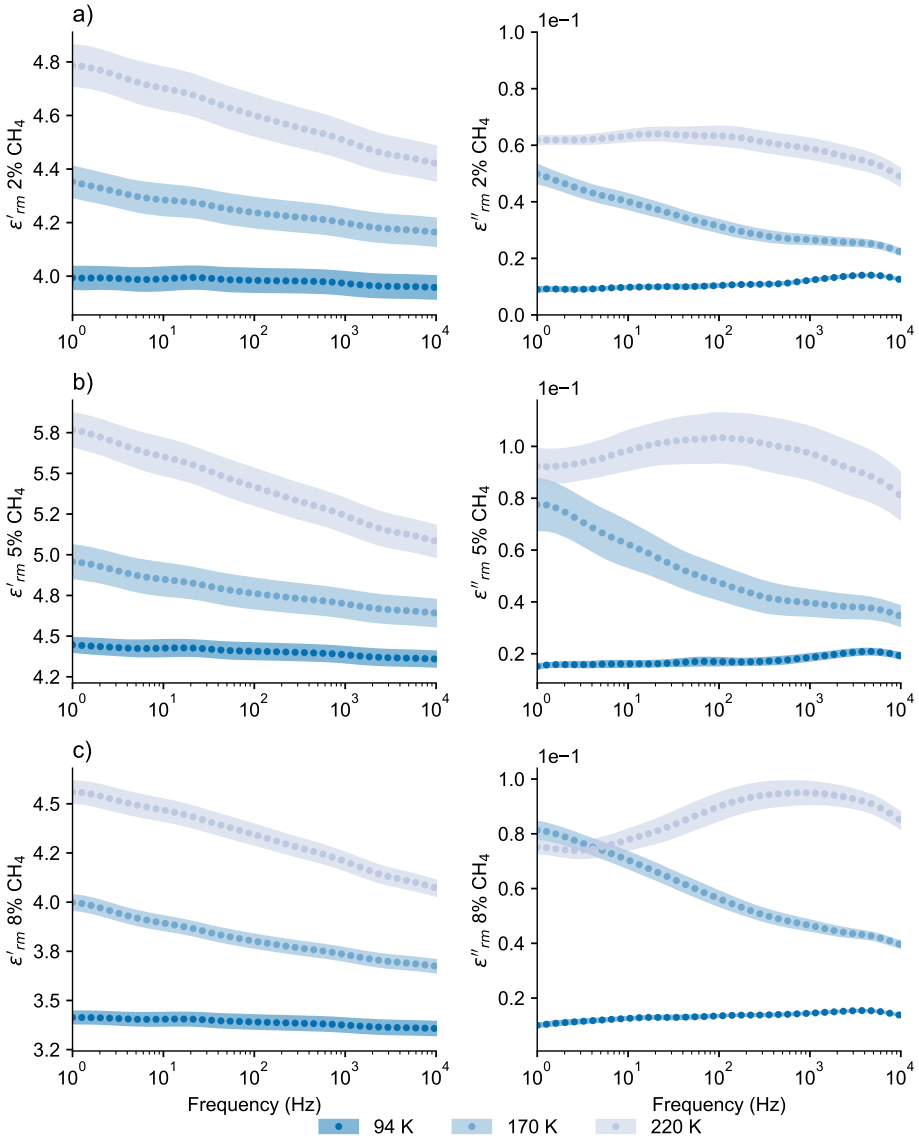

Figure A.3. Real and imaginary parts of the complex permittivity of bulk tholins as a function of frequency for three different temperatures and compositions (2% (a), 5% (b) and 8% (c) of methane in the initial gas mixture).

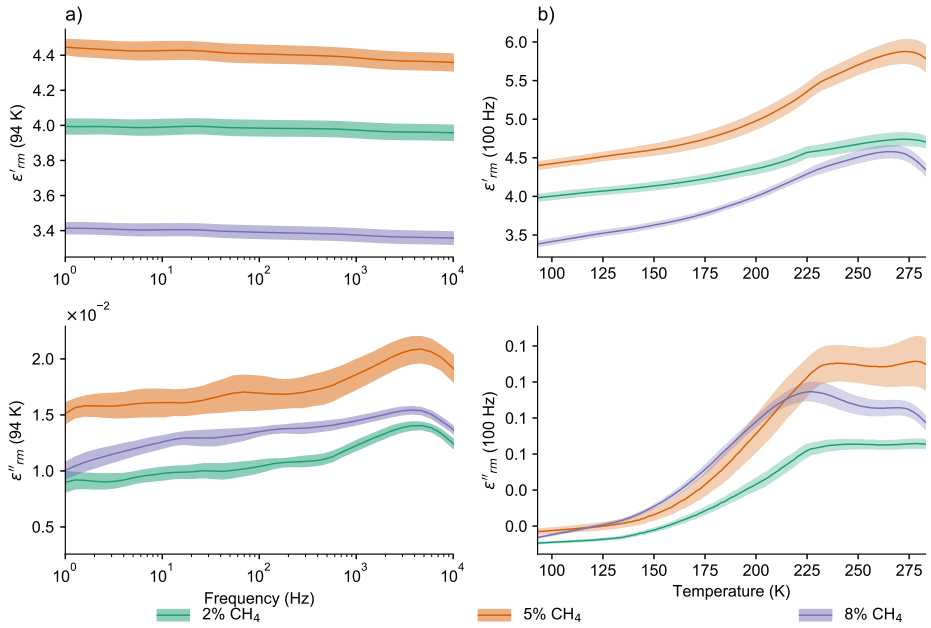

Figure A.4. Frequency (at a temperature of 94 K, column a) and temperature (at a frequency of 100 Hz, column b) dependence and of the real and imaginary parts of the complex permittivity of bulk tholins obtained for 3 gas mixture compositions.

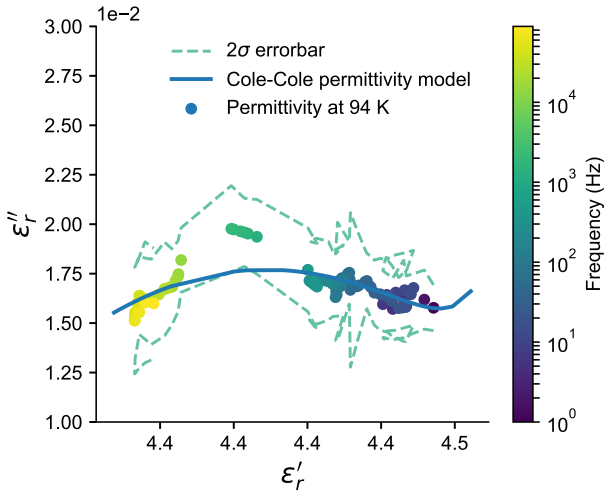

Figure A.5. Complex permittivity at a temperature of 94 K in the complex plane. The best Cole-Cole fit is also represented. The scales for ϵ'_r and ϵ''_r are different in order to provide a readable figure.

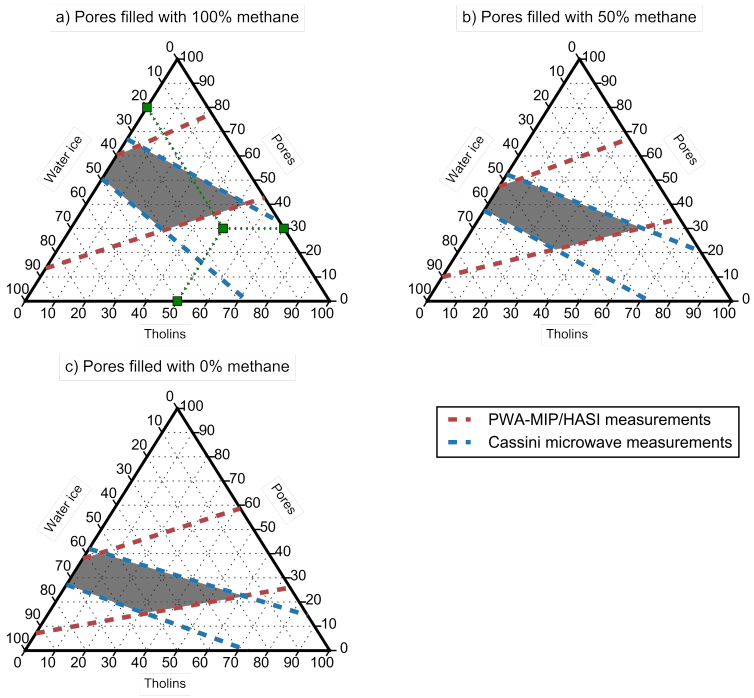

Figure A.6. Ternary diagrams showing the constraints on the composition of the Huygens Landing Site as derived from both PWA-MIP/HASI (red) and the Cassini Radar (blue) observations and assuming that the subsurface pores are saturated with liquid methane (a), half-filled with liquid (b) or empty (c). The intersection of the constraints (gray area) represents the most likely composition of the first meter below the surface of the HLS. To help read this diagram, an example is shown (green squares) on the figure, corresponding to a mixture of 30% pores, 50% tholins, and 20% water ice.

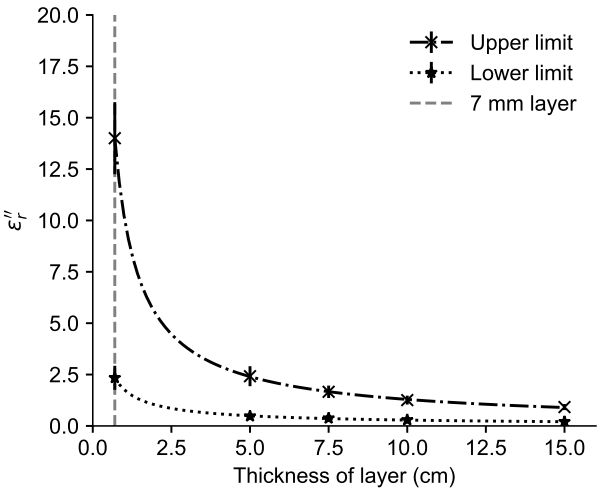

Figure A.7. Upper and lower limits of the imaginary part of the permittivity of the superficial conductive layer required to explain PWA-MIP/HASI measurements. These limits were obtained by using the two extreme cases of the probe attitude at the surface of Titan. The values at 7 mm were extrapolated